Application of dynamic spatiotemporal modeling to predict urban traffic–related air pollution changes

Seyedeh Zeinab Shogrkhodaei[1] · Amanollah Fathnia[1] · Seyed Vahid Razavi-Termeh[2] ·
Sirous Hashemi Dareh Badami[3] · Khalifa M. Al-Kindi[4]

Abstract

Traffic-related urban air pollution is a pressing concern in Tehran, Iran, with severe health implications. This study aimed to create a dynamic spatiotemporal model to predict changes in urban traffic-related air pollution in Tehran using a land use regression (LUR) model. Two datasets were employed to model the spatiotemporal distribution of gaseous traffic-related pollutants—sulfur dioxide (SO_2), nitrogen dioxide (NO_2), and carbon monoxide (CO). The first dataset incorporated remote sensing data, including land surface temperature (LST), the normalized difference vegetation index (NDVI), apparent thermal inertia (ATI), population density, altitude, land use, road density, road length, and distance to highways. The second dataset excluded remote sensing data, relying solely on population density, altitude, land use, road density, road length, and distance to highways. The LUR model was constructed using both datasets at three different buffer distances: 250, 500, and 1000 m. Evaluation based on the R^2 index revealed that the 1000-m buffer distance achieved the highest accuracy. Without remote sensing data, R^2 values for CO, NO_2, and SO_2 pollutants were respectively spring (0.77, 0.79, 0.51), summer (0.59, 0.71, 0.59), and winter (0.41, 0.52, 0.59). With remote sensing data, R^2 values were respectively spring (0.82, 0.84, 0.74), summer (0.72, 0.87, 0.62), and winter (0.53, 0.59, 0.72). Incorporating remote sensing data notably improved the accuracy of modeling CO, NO_2, and SO_2 during all three seasons. The central, southern, and southeastern regions of Tehran consistently exhibited the highest pollutant concentrations throughout the year, while the northern areas maintained comparatively better air quality.

✉ Amanollah Fathnia
a_fathnia@razi.ac.ir

Seyedeh Zeinab Shogrkhodaei
zeinab.shogrkhodaei@gmail.com

Sirous Hashemi Dareh Badami
siroushashemi62@gmail.com

1   Department of Geography, Faculty of Literature
    and Humanities, Razi University, Kermanshah, Iran

2   Department of Computer Science & Engineering
    and Convergence Engineering for Intelligent Drone,
    XR Research Center, Sejong University, Seoul,
    Republic of Korea

3   Department of Geography, Faculty of Literature
    and Humanities, University of Tehran, Tehran, Iran

4   UNESCO Chair of Aflaj Studies, Archaeohydrology,
    University of Nizwa, Nizwa, Oman

Introduction

Owing to the persistence of pollutants in the air, in recent years, air quality has suffered a crisis all over the world (Shogrkhodaei et al. 2021). One of the important environmental issues in large and dense Asian cities is poor air quality (Shi et al. 2021). Air pollution is a complex combination of fine particles and gases (Amini et al. 2019), which causes damage to the health of humans and other living organisms (Kim et al. 2015). Gas, liquid, and solid phase pollutants are among the environmental pollutants that reduce air quality and maintain clean air for present and future life (Xiang et al. 2022). Gaseous pollutants adversely affect people's respiratory health more than PM_{10} or $PM_{2.5}$ (Xu et al. 2022). Gaseous pollutants such as SO_2, NO_2, and CO are emitted mainly from burning fossil fuels in industries and by vehicle engines (Agarwal and Aggarwal 2023).

Rapid urbanization has caused several environmental problems, including increased levels of air pollution that hurt human health and the global climate (Malik et al. 2019). The Middle East's urban population expanded from 35% in 1960 to 65% in 2015, greatly above the global average of 55%, according to the World Bank (El Kenawy et al. 2021). According to the report of the World Health Organization, air pollution caused the death of 2.4 million people worldwide in 2016, of which 91% were in low- and middle-income countries (Chen et al. 2020). According to the results of epidemiologic research, the death rate is higher in cities with severe air pollution. This statistic shows lower rates of death in cities with lower air pollution levels (Amini et al. 2014). Vulnerability to urban air pollution can cause cardiovascular illness, acute respiratory ailments (such as asthma), malignant tumors, and mortality (Fritsch and Behm 2021; Bertazzon et al. 2015; Dirgawati et al. 2015; Saucy et al. 2018). Although air pollution in affluent cities has decreased over time, it remains a major concern for people's health and the environment in developing countries (Wang et al. 2013). The increased use of fossil fuels in transportation, commercial activities, industrial centers, traffic, and heating equipment are just a few of the causes of declining air quality in large cities (Shogrkhodaei et al. 2021). The importance of air pollution modeling grows every day because of the rising concentrations of pollutants in the air and the resulting harm to people's health and the environment (Sahsuvaroglu et al. 2006). Air pollution in Asia is one of the biggest challenges in the region because environmental performance does not match economic progress or environmental development (Atash 2007). Cities such as Tehran and Mashhad are among the most polluted cities in Iran due to industrial centers and heavy urban traffic (Miri et al. 2016).Tehran is considered one of the largest cities in West Asia, which consumes about 20% of the country's energy and faces acute air quality problems.

Air pollution modeling is a useful method for estimating and predicting pollutants as well as assessing their impacts (Rybarczyk and Zalakeviciute 2018). Several methods are commonly used to model air pollution, including dispersion and interpolation models, machine learning (ML), and land use regression (LUR) models (Ryan and LeMasters 2007). To estimate air pollution concentrations, dispersion models are based on deterministic equations that require precise information on the source, topography, diffusion, and chemical and physical properties of pollutants (Klompmaker et al. 2021; Morley and Gulliver 2018). Interpolation-based methods (such as kriging) based on deterministic and stochastic geostatistical techniques are commonly used at regional and national sizes. Furthermore, these approaches do not take into account geography or localized patterns, making them incapable of detecting small-scale spatial changes (Wang et al. 2013). These models cannot fully analyze geographical

variations on small scales when the number of air pollution monitoring stations is minimal (Jerrett et al. 2005; Luo et al. 2021).

Machine learning models (such as random forests, artificial neural networks) must be configured and are displayed as black boxes, which necessitates extensive understanding of algorithms as well as evaluation of prediction performance (Fritsch and Behm 2021). The LUR model describes variations in urban air pollution on a local scale (Tularam et al. 2021). The LUR model is a location-based technique for modeling numerous air contaminants spatiotemporally and spatially (Amini et al. 2014).This model predicts and spatially distributes pollutants in a certain location by utilizing a geographic information system (GIS) and a regression function between pollutant concentration and a set of land use factors (Dong et al. 2021). This model is then applied to areas where pollutant concentrations have not been observed (Klompmaker et al. 2021). The LUR model's merits include high-resolution prediction of air pollutant concentrations (Wang et al. 2013), simple and rapid performance when compared to dispersion models and interpolation approaches (Dons et al. 2014), and its cost-effectiveness (Wang et al. 2013; Meng et al. 2015). Among the studies that have been done in the field of air pollution monitoring using the LUR model in Iran, we can mention the study of Taghavi-Shahri et al. (2020), which used the LUR model and D-STEM (distributed space–time expectation maximization) software to predict the concentration of particulate matter ($PM_{2.5}$) paid in Tehran. Their findings demonstrated that D-STEM is a helpful tool for LUR modeling, particularly for models where monitoring stations are missing a substantial amount of data. Hassanpour Matikolaei et al. (2019) used the LUR model to predict the concentration of CO, NO_2, and $PM_{2.5}$ pollutants in Tehran, and the results of their research were satisfactory. So far, the LUR model has been used to predict particulate matter (Karimi and Shokrinezhad 2021; Miri et al. 2019; Zhang et al. 2018; Zheng et al. 2022; Sanchez et al. 2018), NO_2 (Xu et al. 2019; Weissert et al. 2018; Saucy et al. 2018; Knibbs et al. 2018), CO (Hassanpour Matikolaei et al. 2019), and SO_2 (Son et al. 2018).

The LUR model is affected by the number and location of air pollution monitoring stations, which is an obstacle to conducting air pollution studies using the LUR model (Dong et al. 2021). One of the limitations primarily observed in the studies conducted in Asia and underdeveloped countries is the low number of air pollution monitoring stations, which limits the possibility of showing the distribution of air pollution with high accuracy (Amini et al. 2014). Ground-based observations serve as the fundamental infrastructure for determining air quality by providing essential data on pollutant concentrations and their variations over space and time. These observations are crucial in measuring air pollution levels and play a pivotal role in the functioning of models

and remote sensing techniques. While spaceborne remote sensing and modeling approaches are valuable tools, they are often utilized alongside ground-based observations to complement and fill gaps in coverage. Several studies have emphasized the significance of ground-based observations in air quality monitoring and research. For example, Viana et al. (2015) highlighted the importance of robust ground-based datasets in understanding pollutant emissions, evaluating exposure levels, and formulating effective air quality management strategies. Similarly, Motlagh et al. (2020) underscored the role of ground-based measurements in assessing the spatial distribution of air pollutants, identifying pollution sources, and validating remote sensing observations. Furthermore, Lin et al. (2020) stressed the need for comprehensive ground-based monitoring networks to capture local-scale variations, validate satellite data, and improve air quality modeling accuracy. These studies collectively emphasize that ground-based observations are vital for reliable air quality assessments. Ground monitoring stations provide high-quality data with detailed spatial and temporal resolution, enabling the identification of pollution hotspots, the evaluation of human exposure levels, and the assessment of pollution control measures. Additionally, ground-based measurements help validate and refine remote sensing data, ensuring accurate spatial mapping and regional-scale assessments. While spaceborne remote sensing and modeling techniques offer valuable insights, they often rely on ground-based observations for calibration and validation. Ground monitoring data provide ground truth measurements for satellite-based observations and assist in identifying biases and uncertainties in remote sensing products. Moreover, ground-based measurements help address limitations in spatial coverage, particularly in areas where satellite observations may be limited due to cloud cover or other atmospheric conditions. Some studies that have faced limitations in pollution monitoring stations have used variables such as vegetation about pollutants to increase the quality of the model (Wu et al. 2017). Remote sensing can retrieve information about the media. Remote sensing is a valuable tool for monitoring and temporally managing phenomena on earth (Shogrkhodaei et al. 2021). GIS-based methods to study the spatial distribution of air pollutants are widely used to convert point data to surface data (Mozumder et al. 2013).

In this study, we recognize the foundational role of ground-based observations in air quality monitoring and analysis. Our aim is to integrate both ground-based and remote sensing data to develop a comprehensive understanding of air quality patterns and trends in Tehran Metropolis. By leveraging these datasets together, we enhance our ability to assess air pollution levels, identify contributing factors, and provide valuable information for policymakers, scientists, and future research efforts. By emphasizing the importance of ground-based observations and their complementary relationship with spaceborne remote sensing and modeling techniques, we establish a comprehensive and robust approach to air quality monitoring and analysis. In this study, we employed the LUR model to predict the levels of gaseous pollutants (specifically SO_2, NO_2, and CO) in Tehran by utilizing remote sensing data, including the normalized difference vegetation index (NDVI), land surface temperature (LST), and thermal inertia (ATI). This study is innovative in two ways: (1) spatiotemporal modeling of three gaseous pollutants at the same time using remote sensing variables and comparing it to the scenario when remote sensing data is not used and (2) implementation of the LUR model in Tehran using remote sensing data.

Materials and methods

Methodology

This investigation was carried out in five steps. The first phase was the creation of a spatial database of SO_2, NO_2, and CO pollutants; environmental variables (altitude, land use, population density, and transportation); and remote sensing (NDVI, LST, and ATI). In the second stage, the values of all parameters were determined in buffers (250, 500, and 1000 m) built around the pollution monitoring sites. The multivariate linear regression model was generated in IBM SPSS 19 software in two modes: (1) using remote sensing data and (2) without remote sensing data for each parameter in the third phase. The correctness of the buffers was tested using the R^2 statistic in the fourth stage. In the next step, the mode selected for modeling was applied to the entire study area using ArcGIS10.2 software and regression coefficients. In the last step, R^2 and root-mean-square error (RMSE) coefficients were used to evaluate the modeling in the whole study area.

The study area

Tehran, Iran's capital, is located at 51 17′ and 51 33′ east longitude and 35 36′ and 35 44′ north latitude, with an average elevation of 1200 m above sea level and an area of more than 700 km^2. Tehran has a population of approximately 9 million people, according to the 2017 census (Fuladlu and Altan 2021). The Alborz Mountains, which trap air pollutants, are one of the causes of Tehran's air pollution. These conditions, which are associated with a temperature inversion during the winter seasons, enhance the concentration of pollutants (Motlagh et al. 2021). Additional causes, such as pollution from manufacturing, motorized transportation, and the usage of fossil fuels, have harmed Tehran's air quality (Razavi-Termeh et al. 2021). The research area in Iran

and the locations of 22 air pollution monitoring stations are depicted in Fig. 1.

Materials

Air pollution data

In this research, three gaseous pollutants (SO$_2$, NO$_2$, and CO) were used to model air pollution. SO$_2$, NO$_2$, and CO pollutant data from 22 pollution measurement stations using Tehran Air Quality Control Company (http://airnow.tehran.ir/) were used in this study. Data on air pollution have been prepared as a daily average for the winter, summer, and spring seasons of 2018. Table 1 shows the average pollutant concentrations in the three seasons of spring, summer, and winter. Figure 2 also depicts the graph of all three parameters. The utilization of air pollutant concentrations in this study involved the acquisition of data from two esteemed governmental agencies operating in Iran: the Air Quality Control Company (AQCC) and the Department of Environment (DoE). These agencies play a pivotal role in monitoring and reporting air pollution levels, furnishing measurements encompassing various temporal resolutions, such as hourly averages, daily averages, monthly averages, and annual averages. With a specific focus on three key gaseous pollutants, namely CO in parts per million (ppm), NO$_2$ in parts per billion (ppb), and SO$_2$ in ppb, we procured the requisite concentration data from these agencies.

Environmental and demographic variables

In this study, land use data, traffic, and population density are used as environmental and demographic data. The data used in this study are similar to the studies of Wang et al. (2013) and Hoek et al. (2008). The criteria used and their characteristics are shown in Fig. 3 and Table 4.
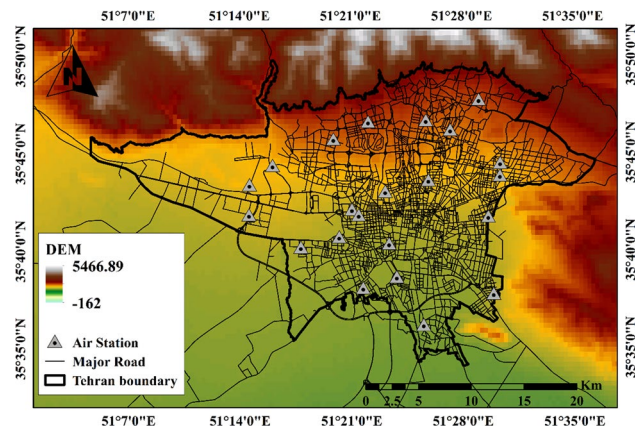
Table 1 The average concentration of pollutants in three seasons: spring, summer, and winter

Pollutants	Spring	Summer	Winter
CO	2.24 ppm	2.41 ppm	2.57 ppm
NO$_2$	44.92 ppb	50.27 ppb	60.86 ppb
SO$_2$	6.08 ppb	6.12 ppb	7.35 ppb

Land use Land use and population are important factors affecting the concentration and intensity of air pollutants in urban areas (Kramer 2013). Impervious surfaces, such as those in residential, industrial, administrative, commercial, and transportation areas, increase air pollution, while green spaces and water bodies can reduce it by absorbing and removing pollutants (Huang et al. 2021). In this study, land use was analyzed using nine categories provided by Tehran Municipality (https://www.tehran.ir), and Arc GIS 10.2 software was used to calculate the values of each land use within the desired buffers.

Population Population density is also a crucial factor, as densely populated areas with more buildings and motor vehicles tend to emit more pollutants related to urban traffic (Dirgawati et al. 2015). Population density data for 2017 Tehran was obtained from the Statistics Organization of Iran (https://www.amar.org.ir), and population density was calculated using Eq. 1, which divides the number of people by the area of each block (measured in km^2):

$$Population\ density = \frac{Number\ of\ people}{Area} \tag{1}$$

The area of each block is expressed in km^2.

Traffic Emissions from motor vehicles are the primary source of air pollution in urban areas (Gonzales et al. 2012).
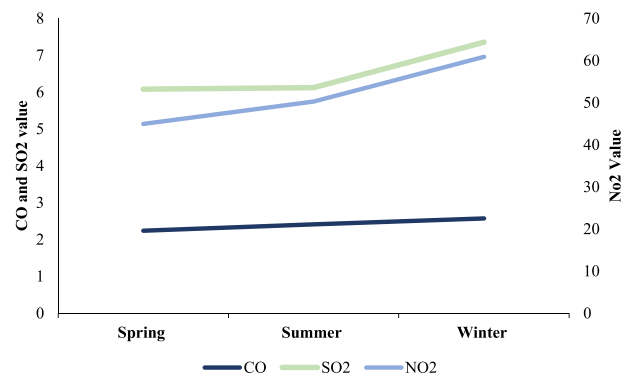

Fig. 1 Location of air pollution monitoring stations in Tehran

Fig. 2 The graph of changes in CO, NO$_2$, and SO$_2$ parameters in three seasons: spring, summer, and winter
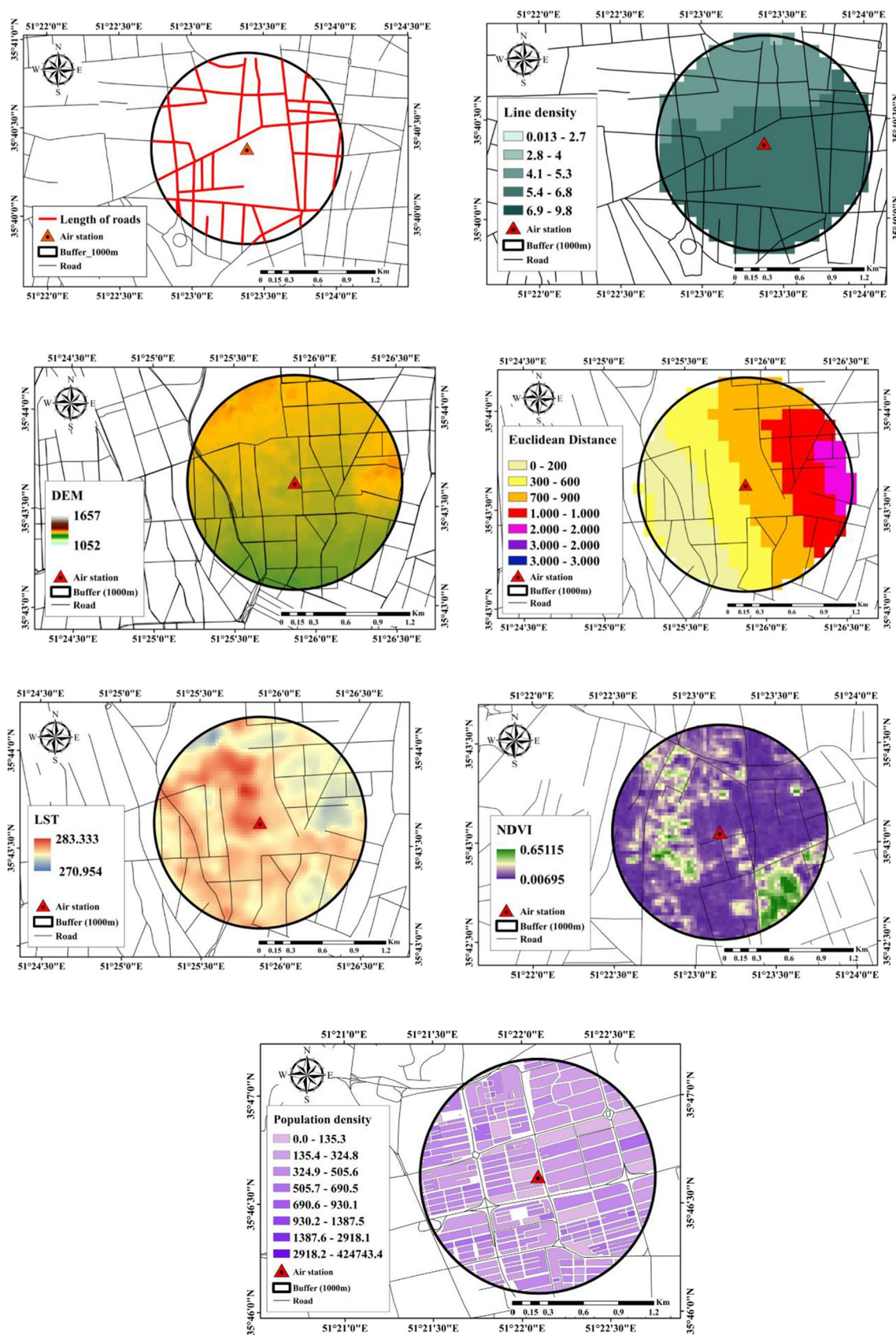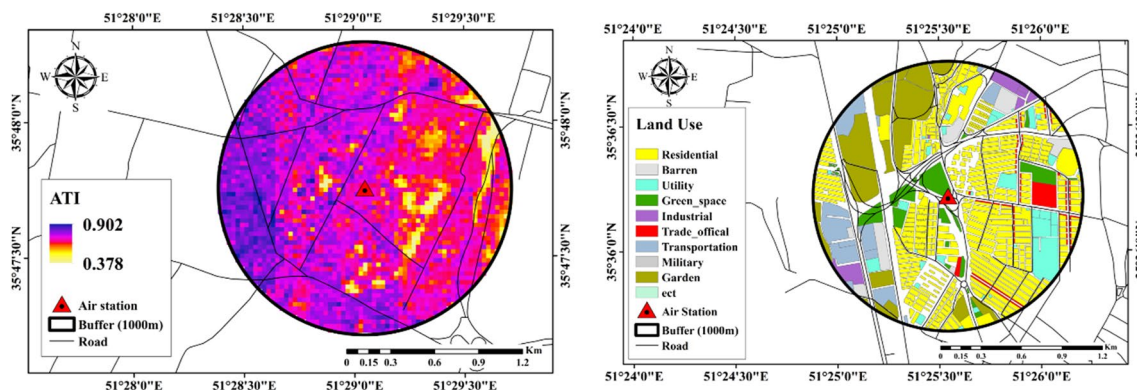
Fig. 3 Map of criteria used in the study

Fig. 3 (continued)

An increase in traffic volume causes an increase in the number of vehicles and ultimately increases the emission of air pollutants (Han and Naeher 2006). Urban traffic data are usually either unavailable or difficult to obtain. In some cities, this information (traffic count) is available only for a small number of streets and mainly on main roads. To solve this problem, it is usually possible to use road density data (Hoek et al. 2008). In this study, owing to the limitations in accessing traffic intensity data, in addition to using alternative variables such as street density, variables such as road length and distance to highways were used to increase accuracy in modeling. Open street map (OSM) (https://www.openstreetmap.org) was used to prepare the road map in 2017 of Tehran city. Density and Euclidean distance analyses were used in ArcGIS 10.2 software to prepare these criteria.

Remote sensing data

Remote sensing data in this study include LST, NDVI, ATI, and DEM (Fig. 3). Studies such as Wong et al. (2021) introduced the use of the NDVI, while Alvarez-Mendoza et al. (2019) and Zeng et al. (2022) investigated LST and ATI. Luminati et al. (2021) employed remote sensing data, specifically NDVI and LST, to model air pollution. Ryu et al. (2019) utilized NDVI as an indicator of live vegetation cover and reduction factor in their LUR model for modeling NO_2 in South Korea, demonstrating that higher NDVI values correspond to decreased NO_2 concentrations. Tian et al. (2019) found that urban areas exhibit higher LST values than suburban areas, while lower NDVI values are observed in urban areas due to the prevalence of impervious surfaces in central urban areas. Zheng et al. (2017) reported a significant positive correlation ($R = 0.67, 0.69, 0.49, 0.46, 0.47$) between LST and various pollutants, including $PM_{2.5}$, PM_{10}, SO_2, NO_2, and CO. Their study also revealed that areas with lower NDVI and higher LST are associated with higher concentrations of these pollutants. Parameters such

as LST, NDVI, and ATI were derived from the integration of MODIS (Terra-Aqua) sensor products with an 8-day and 16-day time resolution and a 1-km spatial resolution and Landsat-8 Enhanced Thematic Mapper Plus (ETM +) with a 30-m spatial resolution. MODIS Conversion Toolkit (MCTK) plugin was installed on ENVI 5.3 software to make necessary corrections. This plugin can identify and read all MODIS products. It also determines the required corrections automatically. In this study, the corrections made include ground reference, determining the coordinate system, and geometric corrections according to the type of product. To extract LST using Landsat-8 satellite, atmospheric and radiometric corrections were first performed in ENVI 5.3 software. Then, the reflectance of red and near-infrared bands was used to calculate NDVI, and radiation was calculated based on it. Then, the radiation of the thermal bands and then the brightness temperature of the thermal bands were calculated. Then, LST was calculated. To increase the spatial resolution, MODIS and Landsat-8 images were merged and averaged. To extract NDVI, 8- and 16-day images of MODIS sensor products (Terra-Aqua) were first prepared. Then, the necessary corrections were applied to the image using the MCTK plugin. Also, ENVI 5.3 software was used to extract NDVI using Landsat-8 satellite images (OLI and TIRS sensors) with a time resolution of 1 month. To automatically calculate NDVI in this software, the NDVI option was used in the Transform section. In the next step, to provide a better spatial resolution of the NDVI obtained from the MODIS sensor, OLI and TIRS sensors were combined in Arc GIS 10.2 software (Amiri et al. 2009). The US Geological Survey (USGS)website (https://www.usgs.gov/) was used to obtain the satellite imagery required for this study in April, July, August, January, and February 2018. The characteristics of the images used are shown in Table 2. ENVI 5.3 software was used to prepare these data. Finally, all the images were downscaling in pixels of 30 * 30 m and used in the modeling process. The data relating to ATI was also prepared from 16-day and 8-day daily and nightly images from the MODIS

Table 2 Number and time of images used in the model

Number of images	Date	Satellite/sensor
5	2018 Jan 01 2018 Feb 02 2018 Apr 20 2018 Jul 25 2018 Aug 26	Landsat-8 Enhanced Thematic Mapper Plus (ETM+)
10, 20	April 2018 July 2018 August 2018 January 2018 February 2018	MODIS (Terra-Aqua) (8-day and 16-day Images)

sensor. The steps of their preparation are the same as the LST product of this sensor.

Land surface temperature (LST) The conversion of vegetated surfaces into impervious surfaces increases the temperature of the Earth's surface, which has many environmental effects. In addition, these changes affect the rate of evaporation, wind turbulence, and absorption of solar radiation and cause changes in visibility in atmospheric conditions near the surface of cities (Feizizadeh and Blaschke 2013). There is a positive correlation between the concentration of urban pollutants and LST (Zheng et al. 2017; Weng and Yang 2006). Retrieving the Earth's surface temperature requires obtaining the Earth's Radiant Power (LSE). NDVI thresholding method was used to calculate LSE (Rajeshwari and Mani 2014). In this method, LSE is extracted using the information collected in visible and near-infrared bands of the OLI sensor (Estimation of Reflectance and Vegetation Indices) and the technique proposed by Jiménez-Muñoz and Sobrino (2008). LST retrieval was performed using the separate window (SW) algorithm. This method is calculated using two thermal bands, usually located in the atmospheric window between 10 and 12 microns (Jiménez-Muñoz et al. 2014). Table 3 shows the coefficients used in the separate window algorithm. The SW algorithm based on the mathematical structure proposed by Sobrino et al. (1997) and applied to sensors by Jiménez-Muñoz and Sobrino (2008) was used according to E. 2:

$$T_s = T_i + c_1\left(T_i - T_j\right) + c_2\left(T_i - T_j\right)^2 + c_0 \\ + \left(c_3 + c_4 w\right)(1 - \varepsilon)\left(c_5 + c_6 w\right)\Delta\varepsilon \tag{2}$$

T_i and T_j are the brightness temperature of the bands used in the algorithm, ε the average radiant energy of the two bands $\varepsilon = 0.5\left(\varepsilon_i + \varepsilon_j\right)$, $\Delta\varepsilon$ the difference in the radiant power of the two bands $\Delta\varepsilon = \left(\varepsilon_i - \varepsilon_j\right)$, W is the amount of atmospheric water vapor content (grams per square centimeter), and C_0 to C_6 are SW coefficients determined from simulated data.

Normalized difference vegetation index (NDVI) Using solar absorption and selective reflection, vegetation can control environmental conditions and energy exchanges and act as an influential factor in air pollution control and an absorber of NO_x and SO_2 (Zheng et al. 2017). The NDVI can be calculated based on the relationship between energy absorption by chlorophyll in the red band and increased energy reflection in the near-infrared band for healthy vegetation (Lenney et al. 1996). NDVI is calculated according to Eq. 3:

$$NDVI = \frac{\rho_{NIR} - \rho_{RED}}{\rho_{NIR} + \rho_{RED}} \tag{3}$$

ρ_{NIR} is the reflection of the near-infrared band (band 5), and ρ_{RED} is the reflection of the red band (band 4).

Apparent thermal inertia (ATI) Thermal inertia is the degree of acceleration required to bring the temperature of a body close to its surroundings or to reach a balanced state. Thermal inertia depends on absorption, specific heat, thermal conductivity, dimensions, and other factors (Price 1985). Objects with high thermal inertia need a longer time to reach thermal equilibrium with their surroundings, but things with low thermal inertia quickly reach equilibrium with their surroundings. ATI parameter was calculated using night and day LST data from MODIS and land surface albedo obtained from Landsat-8 using Eq. 4 (Price 1985):

$$ATI = \frac{1 - Albedo}{T_S day - T_S night} \tag{4}$$

where ATI is the apparent thermal inertia, T_{sday} and T_{snight} are the daytime and nighttime surface temperatures of the Earth. To calculate the ATI, it is necessary to calculate the albedo value of the surface. Several algorithms were presented by Liang (2005) to extract albedo in broadband sensors by combining different bands by matching the corresponding OLI bands with ETM+ sensor bands. The algorithm used to retrieve the OLI sensor albedo from ETM+ bands was used from Eq. 5:

Table 3 Values of the coefficients used in the separate window algorithm

Coefficient	C_0	C_1	C_2	C_3	C_4	C_5	C_6
Value	−0.268	1.378	0.183	54.3	−2.238	−129.2	16.4

$$\alpha_{short} = 0.365\alpha_2 + 0.130\alpha_4 + 0.373\alpha_5 + 0.085\alpha_6 + 0.072\alpha_7 - 0.0018 \tag{5}$$

where a_2, a_4, a_5, a_6, and a_7 are the ground surface reflectance in bands two, four, five, six, and seven of the OLI sensor, respectively.

Altitude The altitude criterion was prepared from the digital elevation model (DEM) of advanced spaceborne thermal emission and reflection radiometer (ASTER) images with a spatial resolution of 30 * 30 m in Google Earth Engine (GEE) (https://earthengine.google.com/).

Methods

Analysis of buffers

To calculate the values of influential variables (land use, altitude, population density, street density, road length, distance to highways, ATI, LST, and NDVI) on air pollutants, buffers of sizes 250, 500, and 1000 were created around each pollution measurement station using ArcGIS 10.2 (Table 4). The selection of the size of the buffers is influenced by the pollutant dispersion patterns (Beelen et al. 2013), which include measures between the most miniature (250 m) and the largest (1000 m) (Fig. 4). Depending on the size of the area and the number of monitoring stations, buffers of 5000, 3000, and 2000 m have been considered in some studies (Meng et al. 2015).
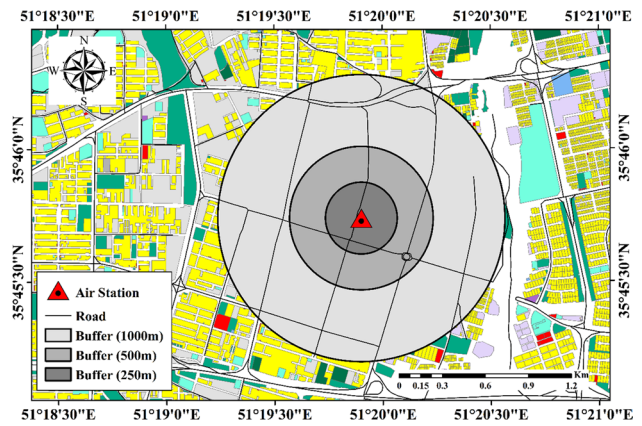

Fig. 4 Display of buffers used in the study

LUR model

The LUR model is a statistical method that describes the relationship between the concentrations measured at air pollution monitoring stations and the influential variables (Amini et al. 2014). The LUR model was first introduced by Briggs et al. (1997) (Beelen et al. 2013). In this study, the LUR model was used to model urban air pollution related to traffic using multivariate linear regression equations. Then, the resulting equation is used to predict the concentrations in the locations that are not measured based on these prediction variables. The linear regression model is calculated with Eq. 6 (Fritsch and Behm 2021):

$$y_i = \beta_0 + \sum_k \beta_{ik} X_{ik} + \varepsilon_i \tag{6}$$

Table 4 Characteristics of data and buffers used in this study

Category	Variable description	Unit	Buffer radius (m)
Land use	Residential	m²	250, 500, 1000
	Transportation	m²	250, 500, 1000
	Agriculture	m²	250, 500, 1000
	Barren	m²	250, 500, 1000
	Green Space	m²	250, 500, 1000
	Industrial	m²	250, 500, 1000
	Military	m²	250, 500, 1000
	Trade official	m²	250, 500, 1000
	Utility	m²	250, 500, 1000
DEM	Digital elevation model	m	250, 500, 1000
Roads	Distance to nearest major road	km	250, 500, 1000
	Length of roads (all)	km	250, 500, 1000
	Road density(all)	km	250, 500, 1000
Population	Population density	(Number)	250, 500, 1000
Satellite data	NDVI	−1 to +1	250, 500, 1000
	LST	Kelvin	250, 500, 1000
	ATI	Kelvin	250, 500, 1000

In this equation, y_i is the interpolated weight at position i, the value of β_0 is the width from the origin, β_{ik} is equal to K the local parameter at ith position, X_{ik} represents the Kth independent variable at ith position, and n represents the previous position (Bertazzon et al. 2015; Henderson et al. 2007).

Model assessment

The LUR model was evaluated using the R^2 and RMSE. The R^2 statistic is related to the ratio of the variance of the dependent variable that can be predicted by the independent variables (Saunders et al. 2012). The R^2 index is calculated according to Eq. 7:

$$R^2 = \frac{\sum_{i=1}^{n}(y_{i-}\widehat{y}_i)}{\sum_{i=1}^{n}(y_{i-}\overline{y})} \tag{7}$$

In this equation, y_i is the observed value of sample i, $\overline{y}$ is the mean of y_i, and $\widehat{y}_i$ is the predicted value of sample i. The closer the R^2 value is to 1, the better the model's performance (Dong et al. 2021).

Results

Performance of the LUR models

The study conducted a comprehensive evaluation of the LUR models using two variants: with remote sensing parameters (NDVI, LST, and ATI) (with RS) and without remote sensing parameters (NDVI, LST, and ATI) (no RS), across three different buffers. The evaluation was conducted across three different buffers: 250 m, 500 m, and 1000 m. Table 5 presents the R^2 values for each pollutant and season, comparing the models with and without remote sensing parameters. Table 5 shows that in spring for CO, the R^2 values increased from 0.68 (no RS) to 0.70 (with RS) at 250 m, 0.72 to 0.77 at 500 m, and 0.77 to 0.82 at 1000 m. Similarly,

for NO_2, the R^2 values improved from 0.57 to 0.61 at 250 m, from 0.68 to 0.76 at 500 m, and from 0.79 to 0.84 at 1000 m. For SO_2, the R^2 values rose from 0.33 to 0.38 at 250 m, from 0.39 to 0.51 at 500 m, and from 0.51 to 0.74 at 1000 m. In the spring season, the incorporation of remote sensing parameters resulted in notable improvements in model performance. In summer, the R^2 values for CO increased from 0.08 to 0.13 at 250 m, from 0.12 to 0.18 at 500 m, and from 0.59 to 0.72 at 1000 m. For NO_2, the R^2 values improved from 0.65 to 0.71 at 250 m, 0.70 to 0.75 at 500 m, and 0.71 to 0.87 at 1000 m. Regarding SO_2, the R^2 values rose from 0.29 to 0.36 at 250 m, 0.37 to 0.46 at 500 m, and 0.59 to 0.62 at 1000 m. During the summer season, the inclusion of remote sensing parameters yielded significant enhancements in the LUR models. In the winter season, for CO, the R^2 values increased from 0.18 to 0.27 at 250 m, from 0.25 to 0.40 at 500 m, and from 0.41 to 0.53 at 1000 m. For NO_2, the R^2 values improved from 0.19 to 0.34 at 250 m, from 0.31 to 0.51 at 500 m, and from 0.52 to 0.59 at 1000 m. Additionally, for SO_2, the R^2 values rose from 0.32 to 0.45 at 250 m, from 0.39 to 0.53 at 500 m, and from 0.59 to 0.72 at 1000 m. In the winter season, the impact of incorporating remote sensing parameters was evident in the improved performance of the LUR models. The numerical results presented in Table 5 demonstrate the positive impact of including remote sensing parameters (NDVI, LST, and ATI) on the performance of the LUR. Consequently, the LUR model was calibrated based on the 1000-m buffer to ensure heightened accuracy in the predictions. To visually illustrate the impact of remote sensing data, Figs. 5 and 6 provide a comprehensive comparison of the model predictions with and without the inclusion of remote sensing parameters for the three pollutants across the three seasons. These figures reinforce the notion that integrating remote sensing parameters into the LUR model enhances its accuracy in predicting air pollutant concentrations. Overall, the results unequivocally suggest that the inclusion of remote sensing parameters, namely, NDVI, LST, and ATI, improves the accuracy of the LUR model. This finding holds true across different seasons and

Table 5 The value of R^2 in three buffers of 250, 500, and 1000 m in two cases: "no RS" without remote sensing indicators and "with RS" considering the selection of remote sensing indicators

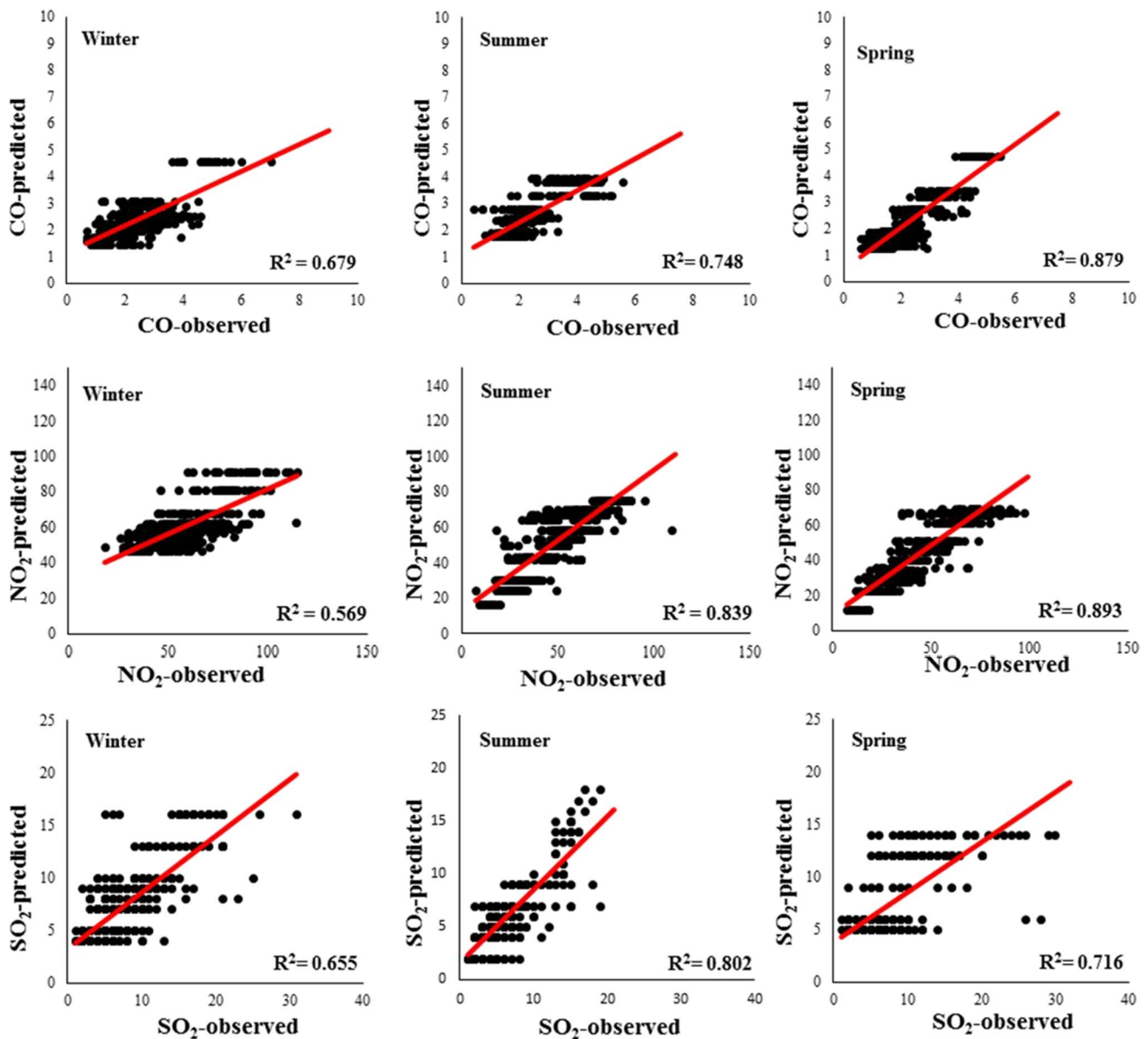|		R^2 (250 m)		R^2 (500 m)		R^2 (1000 m)	
		No RS	With RS	No RS	With RS	No RS	With RS
Spring	CO	0.68	0.70	0.72	0.77	0.77	0.82
	NO_2	0.57	0.61	0.68	0.76	0.79	0.84
	SO_2	0.33	0.38	0.39	0.51	0.51	0.74
Summer	CO	0.08	0.13	0.12	0.18	0.59	0.72
	NO_2	0.65	0.71	0.70	0.75	0.71	0.87
	SO_2	0.29	0.36	0.37	0.46	0.59	0.62
Winter	CO	0.18	0.27	0.25	0.40	0.41	0.53
	NO_2	0.19	0.34	0.31	0.51	0.52	0.59
	SO_2	0.32	0.45	0.39	0.53	0.59	0.72

Fig. 5 Predicted values of CO, NO$_2$, and SO$_2$ parameters without remote sensing data in spring, summer, and winter

is further supported by the selection of the optimal 1000 m buffer for the LUR model calibration. These results signify the valuable contribution of remote sensing data in enhancing the precision and reliability of air pollutant concentration predictions, providing valuable insights for environmental monitoring and decision-making processes.

Spatiotemporal maps of pollutant

Based on the spatiotemporal map presented in Fig. 7, it is observed that the maximum concentration of CO is seen during the winter (2.57 ppm), primarily in the center (roads), east, and southeast regions. During the summer, there is a

decrease in CO concentrations in several northern and northwest areas. The concentrations of NO$_2$ are higher in the winter (60.86 ppb) and have expanded to western locations that exhibited better conditions in the spring and summer. Similarly, the highest concentrations of SO$_2$ are observed in the winter (7.35 ppb), and its geographical changes align with those of CO and NO$_2$. The presence of the Alborz mountain barriers and the west–east movement of the wind likely contribute to higher pollutant concentrations in the central, eastern, southeastern, and southern areas of Tehran compared to the western and northern regions (Fuladlu and Altan 2021; Motlagh et al. 2021). This factor likely caused the pollutants to be trapped next to the Alborz Mountain.
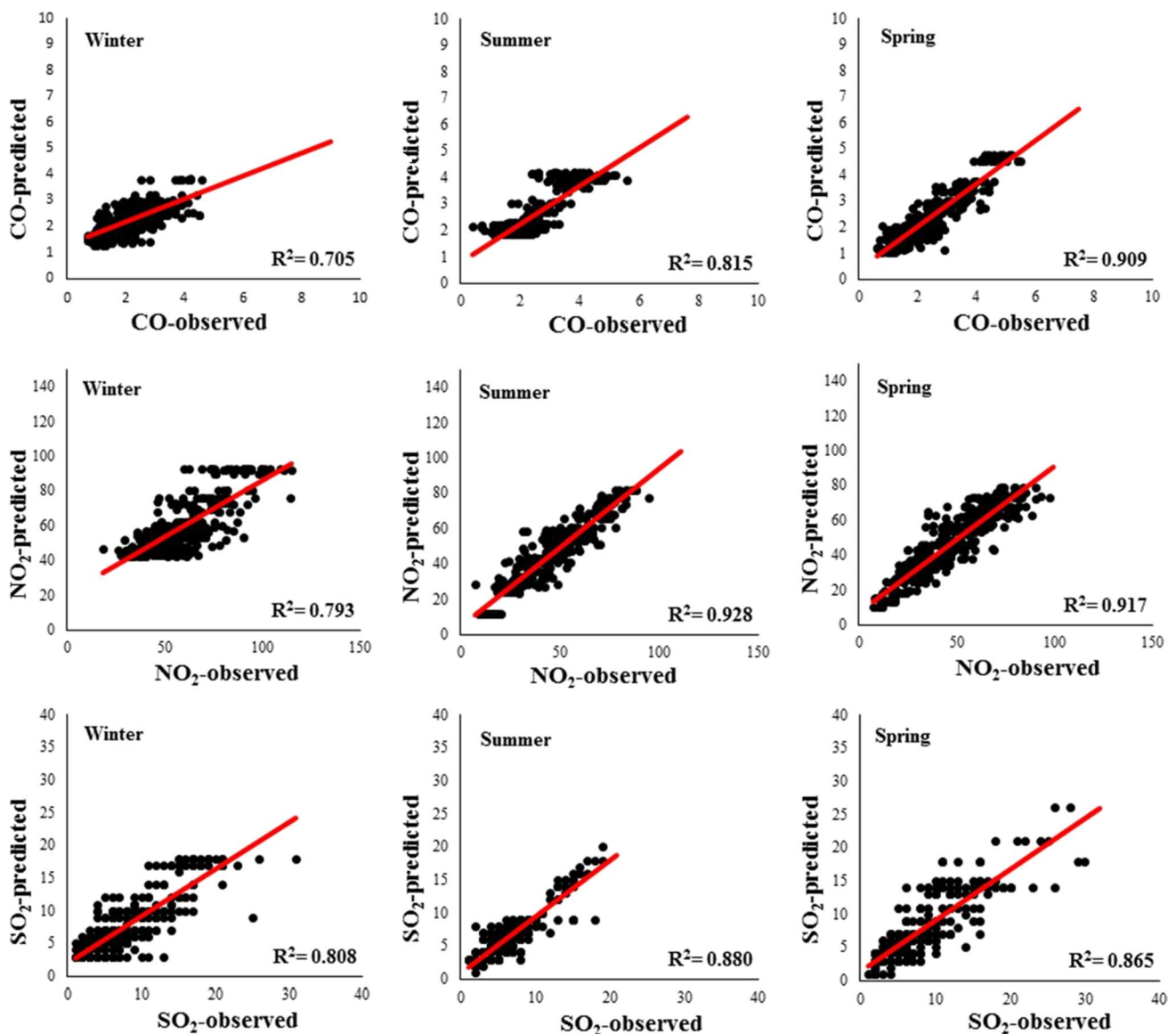
Fig. 6 Predicted values of CO, NO$_2$, and SO$_2$ parameters using remote sensing data in spring, summer, and winter

Discussion

This study aimed to model the spatiotemporal concentrations of SO$_2$, NO$_2$, and CO in Tehran using the LUR model by incorporating remote sensing variables and comparing them to a scenario where remote sensing data was not utilized. By integrating remote sensing variables, such as NDVI, LST, and ATI, into the modeling process, we were able to assess their impact on the accuracy and performance of the LUR models. The results clearly demonstrated that the inclusion of these remote sensing parameters significantly improved the models' ability to predict air pollutant concentrations across different seasons. Notably, the 1000-m buffer consistently exhibited the highest R^2 values for spring (CO: 0.82,

NO$_2$: 0.84, SO$_2$: 0.74), summer (CO: 0.72, NO$_2$: 0.87, SO$_2$: 0.62), and winter (CO: 0.53, NO$_2$: 0.59, SO$_2$: 0.72), indicating its suitability for achieving higher accuracy in the predictions.

Figures 5 and 6 provide a visual comparison between the predictions made with and without the incorporation of remote sensing data for the three pollutants across the three seasons. The observed differences in these comparisons further support our conclusion that integrating remote sensing parameters enhances the accuracy of the LUR model in predicting air pollutant concentrations. Overall, our study highlights the significance of utilizing remote sensing data for modeling spatiotemporal variations in SO$_2$, NO$_2$, and CO concentrations. The inclusion of remote sensing variables
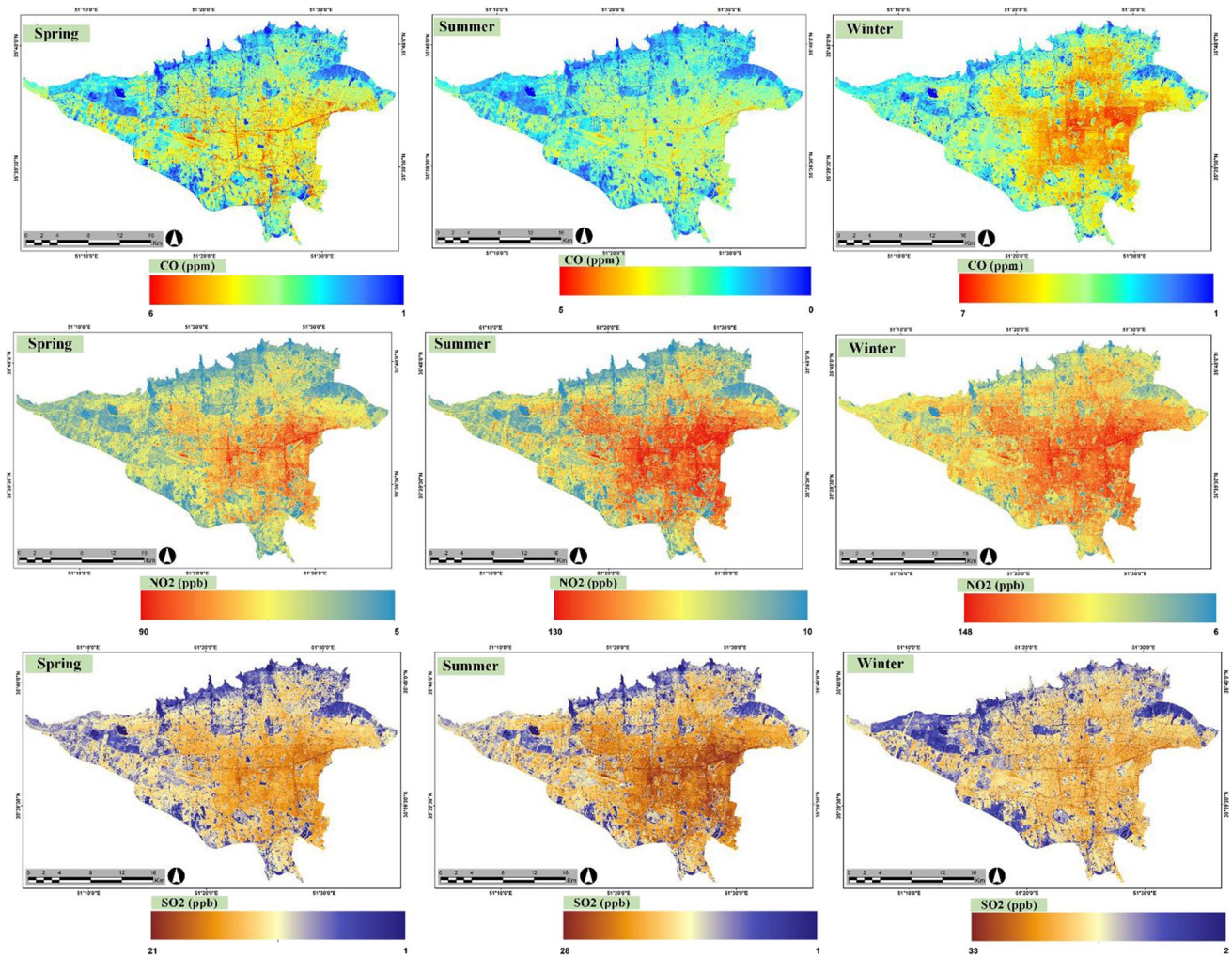
Fig. 7 The spatiotemporal modeling map of CO, NO₂, and SO₂ pollutants

enables a more comprehensive understanding of the air quality dynamics in Tehran and enhances the reliability of the LUR model. This has important implications for environmental monitoring and decision-making processes, providing valuable insights for policymakers and urban planners.

The spatial analysis of the LUR model output maps revealed notable variations in CO concentrations across different seasons. Specifically, higher CO concentrations were observed during winter compared to spring and summer. This can be attributed to factors such as incomplete fuel combustion due to air cooling, the functioning of vehicle emission control systems, and specific climatic conditions during this time of the year, which result in pollutant accumulation on the surface and an overall increase in air pollutant levels (Razavi-Termeh et al. 2021). The reduction of incoming radiation and the shallow boundary layer during winter exacerbate the accumulation of pollutants near the Earth's surface, intensifying air pollution (Zheng et al. 2018). Regarding NO₂ pollutants, their accumulation and

spatial distribution were found to be most prominent during winter compared to spring and summer, with the eastern and central regions exhibiting the highest concentrations. Primary sources of NO₂ emissions include fuel combustion in power plants, vehicles, and heating systems (Matthaios et al. 2019). Several factors contribute to the higher concentration of NO₂ during winter, including the prolonged persistence of NO_x, occurrence of inversion phenomena, increased greenhouse gas levels in the atmosphere, and heightened use of heating devices (Zheng et al. 2018; Gonzales et al. 2012). Future studies should focus on investigating and analyzing the specific causes behind the elevated levels of NO₂ during winter in comparison to summer and spring. In terms of SO₂ concentrations, they were observed to be highest during the winter season compared to other seasons. The spatial distribution of SO₂ closely resembled that of NO₂ and CO, with higher concentrations along communication routes and inner city roads. Factors contributing to increased SO₂ concentrations during winter include higher fossil fuel consumption,

longer atmospheric persistence of SO_2 in cold seasons, emissions from residential heating, and meteorological conditions that promote reduced mixing depth and air stagnation (Li et al. 2022; Lee et al. 2011). Further investigation and analysis are warranted to explore the specific influences and dynamics underlying the elevated levels of SO_2 during the winter season. By unraveling the seasonal patterns and spatial distributions of CO, NO_2, and SO_2 concentrations in Tehran, our study sheds light on the key factors driving air pollution in the region and provides insights for future research and mitigation strategies.

For the strengths of this study, we can mention the use of Landsat 8 satellite data (TIRS/OLI and ETM +) and Terra and Aqua satellites (MODIS instrument), which has increased the performance of the LUR model. R^2 values were used in all cases for SO_2 (spring: 0.74, summer: 0.62, winter: 0.72), NO_2 (spring: 0.84, summer: 0.87, winter: 0.59), and CO (spring: 0.82, summer: 0.72, winter: 0.53) increased. These results show the effectiveness of using remote sensing parameters.

The spatiotemporal modeling of air pollution carried out in this study significantly helps to understand more deeply the release of pollutants at the range level and more accurate planning for prevention and providing valuable solutions. Spatial modeling identifies areas prone to the accumulation of air pollutants, and temporal modeling emphasizes the greater importance of the season, which causes contaminants to persist longer in the atmosphere under the influence of environmental and other variables.

Among the limitations of this study, we can mention the low number of pollution measurement stations. Also, the incompleteness of the data of some stations during the study period caused the modeling accuracy to decrease. One of the critical factors in the concentration of atmospheric pollutants is meteorological conditions and climate variables. These factors, directly and indirectly, affect air quality. But in this study, these critical factors were ignored due to the limited access to meteorological data. Due to the unavailability of traffic data (one of the most critical factors of the LUR model) in this study, alternative variables such as road density, road length, and distance to highways were used. These alternative variables play an essential role in air pollution modeling, but it should be noted that traffic count data is more critical than these alternative variables.

Conclusion

The incorporation of remote sensing data, including LST, the NDVI, and ATI, enhanced the accuracy of the LUR model in predicting SO_2, NO_2, and CO concentrations. The evaluation based on the R^2 index revealed that the 1000-m buffer distance yielded the highest accuracy in predicting pollutant concentrations. The findings demonstrated that including remote sensing data improved the model's performance in all three seasons—spring, summer, and winter—for CO, NO_2, and SO_2 parameters. Moreover, the spatial analysis highlighted that Tehran's central, south, and southeast regions consistently exhibited the highest concentrations of pollutants, while the northern areas generally experienced better air quality. The significance of predicting air quality in Tehran lies in addressing the severe pollution issues and the associated health risks. The findings of this study contribute to the existing knowledge by providing insights into the spatiotemporal patterns of urban traffic-related air pollution and emphasizing the importance of incorporating remote sensing data in dynamic modeling approaches. The results have implications for informed decision-making and policy development to mitigate air pollution and protect public health. Policymakers and stakeholders can utilize the findings to implement targeted measures and interventions to improve air quality in the identified high-concentration areas. The suggestions for future work are as follows: (1) Future research should utilize meteorological data affecting air pollution alongside other variables; (2) using actual traffic count data can increase the power and accuracy of the model; (3) additional monitoring of air pollution parameters using satellite data, such as that provided by Sentinel-5, can improve the model's precision when used in conjunction with data from monitoring stations.

Declarations

References

Agarwal R, Aggarwal SG (2023) A year-round study of ambient gaseous pollutants, their atmospheric chemistry and role in secondary

particle formation at an urban site in Delhi. Atmos Environ 295:119557. https://doi.org/10.1016/j.atmosenv.2022.119557

Alvarez-Mendoza CI, Teodoro AC, Torres N, Vivanco V (2019) Assessment of remote sensing data to model PM10 estimation in cities with a low number of air quality stations: a case of study in Quito. Ecuador Environ 6(7):85. https://doi.org/10.3390/environments6070085

Amini H, Taghavi-Shahri SM, Henderson SB et al (2014) Land use regression models to estimate the annual and seasonal spatial variability of sulfur dioxide and particulate matter in Tehran Iran. Sci Total Environ 488:343–353. https://doi.org/10.1016/j.scitotenv.2014.04.106

Amini H, Nhung NTT, Schindler C et al (2019) Short-term associations between daily mortality and ambient particulate matter, nitrogen dioxide, and the air quality index in a Middle Eastern megacity. Environ Pollut 254:113121. https://doi.org/10.1016/j.envpol.2019.113121

Amiri R, Weng Q, Alimohammadi A, Alavipanah SK (2009) Spatial–temporal dynamics of land surface temperature in relation to fractional vegetation cover and land use/cover in the Tabriz urban area Iran. Remote Sens Environ 113(12):2606–2617. https://doi.org/10.1016/j.rse.2009.07.021

Atash F (2007) The deterioration of urban environments in developing countries: Mitigating the air pollution crisis in Tehran Iran. Cities 24(6):399–409. https://doi.org/10.1016/j.cities.2007.04.001

Beelen R, Hoek G, Vienneau D et al (2013) Development of NO_2 and NOx land use regression models for estimating air pollution exposure in 36 study areas in Europe-The ESCAPE project. Atmos Environ 72:10–23. https://doi.org/10.1016/j.atmosenv.2013.02.037

Bertazzon S, Johnson M, Eccles K, Kaplan GG (2015) Accounting for spatial effects in land use regression for urban air pollution modeling. Spat Spatiotemporal Epidemiol 14:9–21. https://doi.org/10.1016/j.sste.2015.06.002

Briggs DJ, Collins S, Elliott P et al (1997) Mapping urban air pollution using GIS: a regression-based approach. Int J Geogr Inf Sci 11(7):699–718. https://doi.org/10.1080/136588197242158

Chen J, Wang B, Huang S, Song M (2020) The influence of increased population density in China on air pollution. Sci Total Environ 735:139456. https://doi.org/10.1016/j.scitotenv.2020.139456

Dirgawati M, Barnes R, Wheeler AJ et al (2015) Development of land use regression models for predicting exposure to NO_2 and NOx in metropolitan Perth, Western Australia. Environ Model Softw 74:258–267. https://doi.org/10.1016/j.envsoft.2015.07.008

Dong J, Ma R, Cai P et al (2021) Effect of sample number and location on accuracy of land use regression model in NO_2 prediction. Atmos Environ 246:118057. https://doi.org/10.1016/j.atmosenv.2020.118057

Dons E, Van Poppel M, Panis LI et al (2014) Land use regression models as a tool for short, medium and long term exposure to traffic related air pollution. Sci Total Environ 476:378–386. https://doi.org/10.1016/j.scitotenv.2014.01.025

El Kenawy AM, Lopez-Moreno JI, McCabe MF, Domínguez-Castro F, Peña-Angulo D, Gaber IM., …, Vicente-Serrano SM (2021) The impact of COVID-19 lockdowns on surface urban heat island changes and air-quality improvements across 21 major cities in the Middle East. Environ Pollut 288:117802. https://doi.org/10.1016/j.envpol.2021.117802

Feizizadeh B, Blaschke T (2013) Examining urban heat island relations to land use and air pollution: multiple endmember spectral mixture analysis for thermal remote sensing. IEEE J Sel Top Appl Earth Obs Remote Sens 6(3):1749–1756. https://doi.org/10.1109/JSTARS.2013.2263425

Fritsch M, Behm S (2021) Agglomeration and infrastructure effects in land use regression models for air pollution–specification,

estimation, and interpretations. Atmos Environ 253:118337. https://doi.org/10.1016/j.atmosenv.2021.118337

Fuladlu K, Altan H (2021) Examining land surface temperature and relations with the major air pollutants: a remote sensing research in case of Tehran. Urban Clim 39:100958. https://doi.org/10.1016/j.uclim.2021.100958

Gonzales M, Myers O, Smith L et al (2012) Evaluation of land use regression models for $NO2$ in El Paso, Texas, USA. Sci Total Environ 432:135–142. https://doi.org/10.1016/j.scitotenv.2012.05.062

Han X, Naeher LP (2006) A review of traffic-related air pollution exposure assessment studies in the developing world. Environ Int 32(1):106–120. https://doi.org/10.1016/j.envint.2005.05.020

Hassanpour Matikolaei SAH, Jamshidi H, Samimi A (2019) Characterizing the effect of traffic density on ambient CO, $NO2$, and $PM_{2.5}$ in Tehran, Iran: an hourly land-use regression model. Transp Lett 11(8):436–446. https://doi.org/10.1080/19427867.2017.1385201

Henderson SB, Beckerman B, Jerrett M, Brauer M (2007) Application of land use regression to estimate long-term concentrations of traffic-related nitrogen oxides and fine particulate matter. Environ Sci Technol 41(7):2422–2428. https://doi.org/10.1021/es0606780

Hoek G, Beelen R, De Hoogh K et al (2008) A review of land-use regression models to assess spatial variation of outdoor air pollution. Atmos Environ 42(33):7561–7578. https://doi.org/10.1016/j.atmosenv.2008.05.057

Huang D, He B, Wei L et al (2021) Impact of land cover on air pollution at different spatial scales in the vicinity of metropolitan areas. Ecol Indic 132:108313. https://doi.org/10.1016/j.ecolind.2021.108313

Jerrett M, Arain A, Kanaroglou P (2005) A review and evaluation of intraurban air pollution exposure models. J Expo Sci Environ Epidemiol 15(2):185–204. https://doi.org/10.1038/sj.jea.7500388

Jiménez-Muñoz JC, Sobrino JA (2008) Split-window coefficients for land surface temperature retrieval from low-resolution thermal infrared sensors. IEEE Geosci Remote Sens Lett 5(4):806–809. https://doi.org/10.1109/LGRS.2008.2001636

Jiménez-Muñoz JC, Sobrino JA, Skoković D (2014) Land surface temperature retrieval methods from Landsat-8 thermal infrared sensor data. IEEE Geosci Remote Sens Lett 11(10):1840–1843. https://doi.org/10.1109/LGRS.2014.2312032

Karimi B, Shokrinezhad B (2021) Spatial variation of ambient PM2.5 and PM10 in the industrial city of Arak, Iran: a land-use regression. Atmos Pollut Res 12(12):101235. https://doi.org/10.1016/j.apr.2021.101235

Klompmaker JO, Janssen N, Andersen ZJ et al (2021) Comparison of associations between mortality and air pollution exposure estimated with a hybrid, a land-use regression and a dispersion model. Environ Int 146:106306. https://doi.org/10.1016/j.envint.2020.106306

Knibbs LD, Coorey CP, Bechle MJ et al (2018) Long-term nitrogen dioxide exposure assessment using back-extrapolation of satellite-based land-use regression models for Australia. Environ Res 163:16–25. https://doi.org/10.1016/j.envres.2018.01.046

Kramer M (2013) Our built and natural environments : a technical review of the interactions between land use, transportation, and environmental quality. United States Environmental Protection Agency. Washington, D.C. https://rosap.ntl.bts.gov/view/dot/16166

Lee C, Martin RV, Van Donkelaar A et al (2011) SO_2 emissions and lifetimes: estimates from inverse modeling using in situ and global, space-based (SCIAMACHY and OMI) observations. J Geophys Res Atmos 116(D6). https://doi.org/10.1029/2010JD014758

Lenney MP, Woodcock CE, Collins JB, Hamdi H (1996) The status of agricultural lands in Egypt: the use of multitemporal NDVI

features derived from Landsat TM. Remote Sens Environ 56(1):8–20. https://doi.org/10.1016/0034-4257(95)00152-2

Li H, Zhang J, Wen B et al (2022) Spatial-temporal distribution and variation of NO2 and its sources and chemical sinks in Shanxi Province China. Atmosphere 13(7):1096. https://doi.org/10.3390/atmos13071096

Liang S (2005) Quantitative remote sensing of land surfaces (Vol. 30). John Wiley & Sons.

Lin C, Labzovskii LD, Mak HWL, Fung JC, Lau AK, Kenea ST (2020) Observation of PM2.5 using a combination of satellite remote sensing and low-cost sensor network in Siberian urban areas with limited reference monitoring. Atmos Environ 227:117410. https://doi.org/10.1016/j.atmosenv.2020.117410

Luminati O, de Campos BLDA, Flückiger B, Brentani A, Röösli M, Fink G, de Hoogh K (2021) Land use regression modelling of NO2 in Sao Paulo. Brazil Environ Pollut 289:117832. https://doi.org/10.1016/j.envpol.2021.117832

Luo D, Kuang T, Chen YX et al (2021) Air pollution and pregnancy outcomes based on exposure evaluation using a land use regression model: a systematic review. Taiwan J Obstet Gynecol 60(2):193–215. https://doi.org/10.1016/j.tjog.2021.01.004

Malik MN, Khan HH, Chofreh AG et al (2019) Investigating students' sustainability awareness and the curriculum of technology education in Pakistan. Sustainability 11(9):2651. https://doi.org/10.3390/su11092651

Matthaios VN, Kramer LJ, Sommariva R et al (2019) Investigation of vehicle cold start primary NO2 emissions inferred from ambient monitoring data in the UK and their implications for urban air quality. Atmos Environ 199:402–414. https://doi.org/10.1016/j.atmosenv.2018.11.031

Meng X, Chen L, Cai J et al (2015) A land use regression model for estimating the NO2 concentration in Shanghai, China. Environ Res 137:308–315. https://doi.org/10.1016/j.envres.2015.01.003

Miri M, Derakhshan Z, Allahabadi A, Ahmadi E, Conti GO, Ferrante M, Aval HE (2016) Mortality and morbidity due to exposure to outdoor air pollution in Mashhad metropolis Iran the AirQ Model Approach. Environ Res 151:451–457. https://doi.org/10.1016/j.envres.2016.07.039

Miri M, Ghassou Y, Dovlatabadi A et al (2019) Estimate annual and seasonal PM1, PM2.5 and PM10 concentrations using land use regression model. Ecotoxicol Environ Saf 174:137–145. https://doi.org/10.1016/j.ecoenv.2019.02.070

Morley DW, Gulliver J (2018) A land use regression variable generation, modelling and prediction tool for air pollution exposure assessment. Environ Model Softw 105:17–23. https://doi.org/10.1016/j.envsoft.2018.03.030

Motlagh SHB, Pons O, Hosseini SA (2021) Sustainability model to assess the suitability of green roof alternatives for urban air pollution reduction applied in Tehran. Build Environ 194:107683. https://doi.org/10.1016/j.buildenv.2021.107683

Mozumder C, Reddy KV, Pratap D (2013) Air pollution modeling from remotely sensed data using regression techniques. J Indian Soc Remote Sens 41(2):269–277. https://doi.org/10.1007/s12524-012-0235-2

Price JC (1985) On the analysis of thermal infrared imagery: the limited utility of apparent thermal inertia. Remote Sens Environ 18(1):59–73. https://doi.org/10.1016/0034-4257(85)90038-0

Rajeshwari A, Mani ND (2014) Estimation of land surface temperature of Dindigul district using Landsat 8 data. Int J Res Eng Technol 3(5):122–126. https://doi.org/10.15623/ijret.2014.0305025

Razavi-Termeh SV, Sadeghi-Niaraki A, Choi SM (2021) Effects of air pollution in spatio-temporal modeling of asthma-prone areas using a machine learning model. Environ Res 200:111344. https://doi.org/10.1016/j.envres.2021.111344

Ryan PH, LeMasters GK (2007) A review of land-use regression models for characterizing intraurban air pollution exposure.

Inhal Toxicol 19(sup1):127–133. https://doi.org/10.1080/08958370701495998

Rybarczyk Y, Zalakeviciute R (2018) Machine learning approaches for outdoor air quality modelling: a systematic review. Appl Sci 8(12):2570. https://doi.org/10.3390/app8122570

Ryu J, Park C, Jeon SW (2019) Mapping and statistical analysis of NO2 concentration for local government air quality regulation. Sustainability 11(14):3809. https://doi.org/10.3390/su11143809

Sahsuvaroglu T, Arain A, Kanaroglou P (2006) A land use regression model for predicting ambient concentrations of nitrogen dioxide in Hamilton, Ontario Canada. J Air Waste Manag Assoc 56(8):1059–1069. https://doi.org/10.1080/10473289.2006.10464542

Sanchez M, Ambros A, Milà C et al (2018) Development of land-use regression models for fine particles and black carbon in peri-urban South India. Sci Total Environ 634:77–86. https://doi.org/10.1016/j.scitotenv.2018.03.308

Saucy A, Röösli M, Künzli N et al (2018) Land use regression modelling of outdoor NO2 and PM25 concentrations in three low income areas in the western cape province, South Africa. Int J Environ Res Public Health 15(7):1452. https://doi.org/10.3390/ijerph15071452

Saunders LJ, Russell RA, Crabb DP (2012) The coefficient of determination: what determines a useful R^2 statistic? Investig Ophthalmol Vis Sci 53(11):6830–6832. https://doi.org/10.1167/iovs.12-11354

Shi Y, Lau AKH, Ng E et al (2021) A multiscale land use regression approach for estimating intraurban spatial variability of PM2.5 concentration by integrating multisource datasets. Int J Environ Res Public Health 19(1):321. https://doi.org/10.3390/ijerph19010321

Shogrkhodaei SZ, Razavi-Termeh SV, Fathnia A (2021) Spatio-temporal modeling of pm2.5 risk mapping using three machine learning algorithms. Environ Pollut 289:117859. https://doi.org/10.1016/j.envpol.2021.117859

Sobrino JA, Li ZL, Stoll MP, Becker F (1997) Multi-channel and multi-angle algorithms for estimating sea and land surface temperature with ATSR data. Oceanogr Lit Rev 2(44):162–163. https://doi.org/10.1080/01431169608948760

Son Y, Osornio-Vargas ÁR, O'Neill MS et al (2018) Land use regression models to assess air pollution exposure in Mexico City using finer spatial and temporal input parameters. Sci Total Environ 639:40–48. https://doi.org/10.1016/j.scitotenv.2018.05.144

Taghavi-Shahri SM, Fassò A, Mahaki B, Amini H (2020) Concurrent spatiotemporal daily land use regression modeling and missing data imputation of fine particulate matter using distributed space-time expectation maximization. Atmos Environ 224:117202. https://doi.org/10.1016/j.atmosenv.2019.117202

Tian Y, Yao X, Chen L (2019) Analysis of spatial and seasonal distributions of air pollutants by incorporating urban morphological characteristics. Comput Environ Urban Syst 75:35–48. https://doi.org/10.1016/j.compenvurbsys.2019.01.003

Tularam H, Ramsay LF, Muttoo S (2021) A hybrid air pollution/land use regression model for predicting air pollution concentrations in Durban South Africa. Environ Pollut 274:116513. https://doi.org/10.1016/j.envpol.2021.116513

Wang R, Henderson SB, Sbihi H et al (2013) Temporal stability of land use regression models for traffic-related air pollution. Atmos Environ 64:312–319. https://doi.org/10.1016/j.atmosenv.2012.09.056

Weissert LF, Salmond JA, Miskell G et al (2018) Development of a microscale land use regression model for predicting NO2 concentrations at a heavy trafficked suburban area in Auckland, NZ. Sci Total Environ 619:112–119. https://doi.org/10.1016/j.scitotenv.2017.11.028

Weng Q, Yang S (2006) Urban air pollution patterns, land use, and thermal landscape: an examination of the linkage using GIS. Environ Monit Assess 117(1):463–489. https://doi.org/10.1007/s10661-006-0888-9

Wu CD, Chen YC, Pan WC et al (2017) Land-use regression with long-term satellite-based greenness index and culture-specific sources to model PM2.5 spatial-temporal variability. Environ Pollut 224:148–157. https://doi.org/10.1016/j.envpol.2017.01.074

Xiang W, Yuan J, Wu Y, Luo H, Xiao C, Zhong N, … & He Y (2022) Working principle and application of photocatalytic optical fibers for the degradation and conversion of gaseous pollutants. Chin Chem Lett 33(8):3632–3640. https://doi.org/10.1016/j.cclet.2021.11.074

Xu H, Bechle MJ, Wang M et al (2019) National $PM_{2.5}$ and NO_2 exposure models for China based on land use regression, satellite measurements, and universal kriging. Sci Total Environ 655:423–433. https://doi.org/10.1016/j.scitotenv.2018.11.125

Xu H, Wang X, Tian Y, Tian J, Zeng Y, Guo Y, … & Feng G (2022) Short-term exposure to gaseous air pollutants and daily hospitalizations for acute upper and lower respiratory infections among children from 25 cities in China. Environ Res 212:113493. https://doi.org/10.1016/j.envres.2022.113493

Zeng L, Hang J, Wang X, Shao M (2022) Influence of urban spatial and socioeconomic parameters on $PM_{2.5}$ at subdistrict level: a land use regression study in Shenzhen China. J Environ Sci 114:485–502. https://doi.org/10.1016/j.jes.2021.12.002

Zhang Z, Wang J, Hart JE et al (2018) National scale spatiotemporal land-use regression model for $PM_{2.5}$, PM_{10} and NO_2 concentration in China. Atmos Environ 192:48–54. https://doi.org/10.1016/j.atmosenv.2018.08.046

Zheng S, Zhou X, Singh RP, Wu Y, Ye Y, Wu C (2017) The spatiotemporal distribution of air pollutants and their relationship with land-use patterns in Hangzhou city China. Atmosphere 8(6):110. https://doi.org/10.3390/atmos8060110

Zheng C, Zhao C, Li Y et al (2018) Spatial and temporal distribution of NO_2 and SO_2 in Inner Mongolia urban agglomeration obtained from satellite remote sensing and ground observations. Atmos Environ 188:50–59. https://doi.org/10.1016/j.atmosenv.2018.06.029

Zheng S, Zhang C, Wu X (2022) Estimating PM2. 5 concentrations using an improved land use regression model in Zhejiang China. Atmosphere 13(8):1273. https://doi.org/10.3390/atmos13081273